Bulletin of the Seismological Society of America, Vol. 84, No. 5, pp. 1456–1472, October 1994

An Efficient Method for Computing Green's Functions for a Layered Half-Space with Sources and Receivers at Close Depths

by Yoshiaki Hisada

Abstract We propose an analytical method to compute efficiently the displacement and stress of static and dynamic Green's functions for viscoelastic layered half-spaces. When source and receiver depths are close, it is difficult to compute Green's functions of the layered half-space, because their integrands, whose variable of integration is the horizontal wavenumber, oscillate with only slowly decreasing amplitude. In particular, when the depths are equal, it is extremely difficult to compute the stress Green's functions, because their integrands oscillate with increasing amplitude. To remedy this problem, we first derive the asymptotic solutions, which converge to the integrands of Green's functions with increasing wavenumber. For this purpose, we modify the generalized R/T (reflection and transmission) coefficient method (Luco and Apsel; 1983) to be completely free from growing exponential terms, which are the obstacles to finding the asymptotic solutions. By subtracting the asymptotic solutions from the integrands of the corresponding Green's functions, we obtain integrands that converge rapidly to zero. We can, therefore, significantly reduce the range of wavenumber integration. Since the asymptotic solutions are expressed by the products of Bessel functions and simple exponential functions, they are analytically integrable. Finally, we obtain accurate Green's functions by adding together numerical and analytical integrations. We first show this asymptotic technique for Green's functions due to point sources, and extend it to Green's functions due to dipole sources. Finally, we demonstrate the validity and efficiency of our method for various cases.

Introduction (Description of the Problem Using a Spherical Wave)

We first explain why there are difficulties in computing the displacement and stress Green's functions, when the source depth is equal or close to the receiver depth. We illustrate this problem with a spherical wave, noting that any 3D wave field can be expressed as a superposition of spherical waves via Huygen's principle. A dynamic spherical wave can be decomposed into cylindrical waves using the Sommerfeld integral (see, e.g., Aki and Richards, 1980)

$$\frac{1}{R}\exp\left(i\frac{\omega}{c}R\right) = \int_0^\infty \left[\frac{k}{\nu}\exp\{-\nu|z-h|\}\,J_0(kr)\right]dk$$

$$R = \sqrt{r^2+(z-h)^2},\ \nu^2 = k^2 - \left(\frac{\omega}{c}\right)^2,\ Re(\nu) \geqq 0, \quad (1)$$

where h and z are the depths of source and receiver, respectively, r is the horizontal distance between the source and the receiver, c is the velocity of the medium, ω is the circular frequency, J_0 is the Bessel function of the order 0, and the variable of integration (k) represents the horizontal wavenumber. In order to obtain stresses, we need to differentiate equation (1) with respect to z or r. For example, the derivative of equation (1) with respect to r gives us

$$\left(\frac{1}{R} - i\frac{\omega}{c}\right)\frac{r}{R^2}\exp\left(i\frac{\omega}{c}R\right) = \int_0^\infty \left[\frac{k^2}{\nu}\exp\{-\nu|z-h|\}\,J_1(kr)\right]dk. \quad (2)$$

When the source depth is equal to the receiver depth ($h = z$), equations (1) and (2) are expressed as

$$\frac{1}{r}\exp\left(i\frac{\omega}{c}r\right) = \int_0^\infty \left\{\frac{k}{\nu}J_0(kr)\right\}dk \tag{3}$$

$$\left(\frac{1}{r} - i\frac{\omega}{c}\right)\frac{1}{r}\exp\left(i\frac{\omega}{c}r\right) = \int_0^\infty \left\{\frac{k^2}{\nu}J_1(kr)\right\}dk, \tag{4}$$

respectively. The integrations here are more difficult to compute than those of equations (1) and (2), because the decaying exponentials ($\exp\{-\nu|z-h|\}$) of equations (1) and (2) disappear and their integrands oscillate with slowly decreasing and increasing amplitudes, respectively, with wavenumber.

The same problem occurs when computing the Green's function of the layered half-space, as described in Apsel and Luco (1983), Herrmann and Wang (1985), Chang (1988), and Herrmann (1993). In order to remedy this problem, two techniques have been proposed. Chang (1988) proposed "the repeated averaging method," taking advantage of the well-behaved damped-oscillating property of the latter part of the integrand of the displacement. This method is stable but is rather time-consuming because a set of accurate peak and trough values in the damped-oscillating part are required to determine the average value. For computing the stress, this method is probably unstable because of the increasing-oscillating property. An alternative, more analytical, method is proposed by Apsel and Luco (1983), who take advantage of the fact that the integrand of the dynamic Green's function converges to that of the static Green's function with increasing k.

We shall explain Apsel and Luco's (1983) idea using our example. The static solutions corresponding to equations (1) and (2) are expressed as follows, by imposing $\omega = 0$

$$\frac{1}{R} = \int_0^\infty [\exp\{-k|z-h|\}J_0(kr)]dk \tag{5}$$

$$\frac{r}{R^3} = \int_0^\infty [k\exp\{-k|z-h|\}J_1(kr)]dk. \tag{6}$$

It is clear that the integrands in equations (1) and (2) approach those in equations (5) and (6) as k increases. Therefore, subtracting equations (5) and (6) from equations (1) and (2) and rearranging, we have

$$\frac{1}{R}\exp\left(i\frac{\omega}{c}R\right) = \int_0^\infty \left[\left\{\frac{k}{\nu}\exp\{-\nu|z-h|\} - \exp\{-k|z-h|\}\right\}J_0(kr)\right]dk + \frac{1}{R} \tag{7}$$

$$\left(\frac{1}{R} - i\frac{\omega}{c}\right)\frac{r}{R^2}\exp\left(i\frac{\omega}{c}R\right) = \int_0^\infty \left[\left\{\frac{k}{\nu}\exp\{-\nu|z-h|\} - \exp\{-k|z-h|\}\right\}kJ_1(kr)\right]dk + \frac{r}{R^3}, \tag{8}$$

respectively. The above integrands quickly converge to zero with wavenumber, even for $h = z$. In fact, when h is equal to z, equations (7) and (8) become

$$\frac{1}{r}\exp\left(i\frac{\omega}{c}r\right) = \int_0^\infty \left[\left\{\frac{k}{\nu} - 1\right\}J_0(kr)\right]dk + \frac{1}{r} \tag{9}$$

$$\left(\frac{1}{r} - i\frac{\omega}{c}\right)\frac{1}{r}\exp\left(i\frac{\omega}{c}r\right) = \int_0^\infty \left[\left\{\frac{k}{\nu} - 1\right\}kJ_1(kr)\right]dk + \frac{1}{r^2}. \tag{10}$$

We find the { } parts in the above integrands converge to zero with increasing k. Thus, we can significantly reduce the integration ranges as compared with those of equations (1) and (2), particularly when the source depth is the same or close to the receiver depth.

The main problem with this method is that there is no analytic integral solution of the static part of the Green's function for a general multi-layered half-space. Apsel and Luco (1983) approximate this by the static solution of the homogeneous half-space with the same material properties as the layer that includes the source, although the convergence is slow. Herrmann and Wang (1985) and Herrmann (1993) improved Apsel and Luco's method by finding numerically approximate asymptotic solutions using Haskell's propagator matrix.

The purpose of this study is to develop Apsel and Luco's (1983) method by finding theoretically appropriate asymptotic solutions. To do this, we first derive integrands of the static and dynamic Green's functions without the growing exponentials, which hinder analytical formation of the asymptotic solutions. Second, we describe the procedure for computing Green's functions due to point and dipole sources. Finally, we check the validity of our method using a layered half-space model.

An Efficient Method to Compute Green's Functions of Layered Half-Space

Static and Dynamic Green's Functions Due to Point Sources

In order to find an analytic form for the asymptotic solutions of the integrands of Green's functions, we need static and dynamic Green's functions that do not have growing exponential terms. For this purpose, we adopt

the generalized R/T (reflection and transmission) coefficient method (Luco and Apsel, 1983) and the stress discontinuity representations (Harkrider, 1964; Haskell, 1964) to express the boundary and source conditions, respectively. The R/T coefficient method is well known to be much more numerically stable than other conventional propagator matrix methods (e.g., Haskell, 1953), because it avoids growing exponential terms by introducing the R/T coefficients of the up/downgoing waves in each layer. Kennett (1974) and Kennett and Kerry (1979) first proposed this method for 2D and 3D cases, respectively. In this study, however, we adopt the other version of the R/T coefficient method by Luco and Apsel (1983), because of the following two reasons. First, its form is simplified by introducing "the generalized R/T coefficient," and its physical meaning is clearly understood. Second, they derived the explicit static solution of the R/T coefficient. The static solution requires consideration of the singularity of the coefficient matrix, which is caused by the disappearance of differences between terms associated with P and S waves. Because of this simplicity, together with the numerical stability up to very high frequencies, the generalized R/T coefficient method by Luco and Apsel (1983) has been widely used to compute not only Green's functions (e.g., Chang, 1988; Chin, 1992) but also the normal modes solution (Chen, 1993). However, Luco and Apsel's formulation includes growing exponentials in the source terms and has numerical instabilities at very high frequencies and/or large wavenumbers. To avoid this problem, we adopt "stress discontinuities" to express the source conditions, as shown by Kennett and Kerry (1979), and derive Green's functions without exponentials growing with wavenumber and/or frequency.

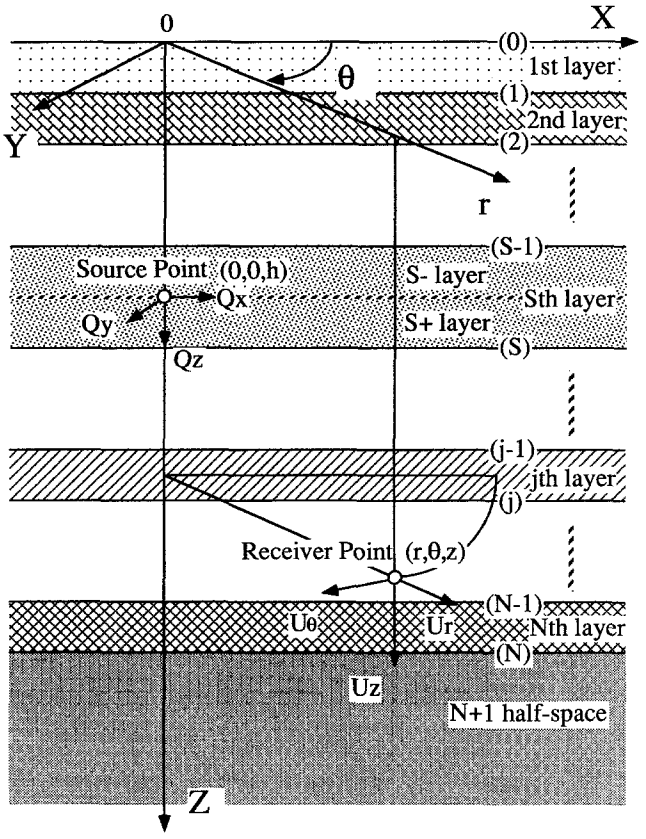

Figure 1. The multi-layered half-space model considered in this study. Point sources are located at (0,0,h) in the sth layer, with the vector components (Q_x,0,0), (0,Q_y,0), and (0,0,Q_z) in the Cartesian coordinate system. The receiver is located at (r,θ,z) in the jth layer, with the displacement components (U_r,U_θ,U_z) in the cylindrical coordinate system.

Figure 1 shows a layered half-space consisting of horizontally flat N layers overlying the homogeneous half-space. Point sources and a receiver are located at (0,0,h) and (r,θ,z), respectively, in the cylindrical coordinate system. We assign the layers with the source and the receiver to the sth and jth layers, respectively. Assuming the time-dependent term as $\exp(-i\omega t)$, static and dynamic Green's functions at the receiver will be the following forms:

$$U^j_{r\binom{x}{y}}(r,\theta,z;h) = \int_0^\infty \left\{ V^j_{1\binom{x}{y}}(z;h)\frac{dJ_1(kr)}{dkr} + H^j_{1\binom{x}{y}}(z;h)\frac{J_1(kr)}{kr}\right\} dk \begin{pmatrix}\cos\theta\\ \sin\theta\end{pmatrix} \equiv u^j_{r\binom{x}{y}}(r,z;h)\begin{pmatrix}\cos\theta\\ \sin\theta\end{pmatrix}$$

$$U^j_{rz}(r,\theta,z;h) = -\int_0^\infty \{V^j_{1z}(z;h)\,J_1(kr)\}dk$$

$$U^j_{\theta\binom{x}{y}}(r,\theta,z;h) = \begin{pmatrix}-\\ +\end{pmatrix}\int_0^\infty \left\{ V^j_{1\binom{x}{y}}(z;h)\frac{J_1(kr)}{kr} + H^j_{1\binom{x}{y}}(z;h)\frac{dJ_1(kr)}{dkr}\right\} dk \begin{pmatrix}\sin\theta\\ \cos\theta\end{pmatrix} \equiv \begin{pmatrix}-\\ +\end{pmatrix} u^j_{\theta\binom{x}{y}}(r,z;h)\begin{pmatrix}\sin\theta\\ \cos\theta\end{pmatrix}$$

$$U^j_{\theta z}(r,\theta,z;h) = 0$$

$$U^j_{z\binom{x}{y}}(r,\theta,z;h) = -\int_0^\infty \left\{ V^j_{2\binom{x}{y}}(z;h)J_1(kr)\right\} dk \begin{pmatrix}\cos\theta\\ \sin\theta\end{pmatrix} \equiv -u^j_{z\binom{x}{y}}(r,z;h)\begin{pmatrix}\cos\theta\\ \sin\theta\end{pmatrix}$$

$$U^j_{zz}(r,\theta,z;h) = -\int_0^\infty \{V^j_{2z}(z;h)\, J_0(kr)\}dk. \tag{11}$$

for displacement, and

$$\sigma^j_{rz\binom{x}{y}}(r,\theta,z;h) = \int_0^\infty \left\{ V^j_{3\binom{x}{y}}(z;h) \frac{dJ_1(kr)}{dkr} + H^j_{2\binom{x}{y}}(z;h) \frac{J_1(kr)}{kr} \right\} dk \begin{pmatrix} \cos\theta \\ \sin\theta \end{pmatrix}$$

$$\sigma^j_{rzz}(r,\theta,z;h) = -\int_0^\infty \{V^j_{3z}(z;h)\, J_1(kr)\}dk$$

$$\sigma^j_{\theta z\binom{x}{y}}(r,\theta,z;h) = \begin{pmatrix} - \\ + \end{pmatrix} \int_0^\infty \left\{ V^j_{3\binom{x}{y}}(z;h) \frac{J_1(kr)}{kr} + H^j_{2\binom{x}{y}}(z;h) \frac{dJ_1(kr)}{dkr} \right\} dk \begin{pmatrix} \sin\theta \\ \cos\theta \end{pmatrix}$$

$$\sigma^j_{\theta zz}(r,\theta,z;h) = 0$$

$$\sigma^j_{zz\binom{x}{y}}(r,\theta,z;h) = -\int_0^\infty \left\{ V^j_{4\binom{x}{y}}(z;h)\, J_1(kr) \right\} dk \begin{pmatrix} \cos\theta \\ \sin\theta \end{pmatrix}$$

$$\sigma^j_{zzz}(r,\theta,z;h) = -\int_0^\infty \{V^j_{4z}(z;h)\, J_0(kr)\}dk \tag{12}$$

for stress. In the above equations, U_r, U_θ, and U_z are the components of displacements in the cylindrical coordinate system, and σ_{rz}, $\sigma_{\theta z}$, and σ_{zz} are those of stresses on the plane normal to the z axis. The superscript j represents the jth layer, and the last subscripts x, y, and z correspond to the solutions due to the point sources with vector components (Q_x, 0, 0), (0, Q_y, 0), and (0, 0, Q_z) in the Cartesian coordinate system, respectively. Within the parentheses, the upper and lower values are allotted to the solutions due to Q_x and Q_y. J_0 and J_1 are Bessel functions of orders 0 and 1, and the variable of integration (k) represents horizontal wavenumber. H^j_1 and H^j_2 and $V^j_1 - V^j_4$ are "the displacement-stress vectors" (Kennett and Kerry, 1979; "the motion-stress vectors" in Aki and Richards, 1980; "vertically polarized waves" in Luco and Apsel, 1983) for *SH* and *P-SV* waves, respectively, which depend on z, h, k, and the source and boundary conditions. The explicit forms of the displacement-stress vectors, which do not have growing exponentials, are given in Appendix A.

Asymptotic Solution of Green's Function

We find the asymptotic solutions of Green's functions at large wavenumbers. Since our main concern is the case when the source depth is equal or close to the receiver depth, we assume the source and the receiver are located in the same jth layer for the derivation of our equations. Later, we shall numerically check the validity of these equations for the cases when the source and/or the receiver are located on a boundary between layers and/or in different layers. As shown in Appendix B, the displacement-stress vectors for very large k converge to the following forms:

$$H^j_{1q}(z;h) \approx \tilde{H}^j_{1q}(z;h) = \tilde{H}^j_{1q} \exp\{-k|z-h|\}$$

$$\begin{Bmatrix} V^j_{1q}(z;h) \\ V^j_{2q}(z;h) \end{Bmatrix} \approx \begin{Bmatrix} \tilde{V}^j_{1q}(z;h) \\ \tilde{V}^j_{2q}(z;h) \end{Bmatrix} = \begin{Bmatrix} \tilde{V}^j_{11q} + k\tilde{V}^j_{12q} \\ \tilde{V}^j_{21q} + k\tilde{V}^j_{22q} \end{Bmatrix} \exp\{-k|z-h|\},$$

$$(q = x, y, \text{ or } z)$$

$$\tilde{V}^j_{12q} = \tilde{V}^j_{22q} = 0, \text{ for } z = h \tag{13}$$

for the displacement vectors, and

$$H^j_{2q}(z;h) \approx \tilde{H}^j_{2q}(z;h) = \tilde{H}^j_{2q} k \exp\{-k|z-h|\}$$

$$\begin{Bmatrix} V^j_{3q}(z;h) \\ V^j_{4q}(z;h) \end{Bmatrix} \approx \begin{Bmatrix} \tilde{V}^j_{3q}(z;h) \\ \tilde{V}^j_{4q}(z;h) \end{Bmatrix} = \begin{Bmatrix} \tilde{V}^j_{31q} + k\tilde{V}^j_{32q} \\ \tilde{V}^j_{41q} + k\tilde{V}^j_{42q} \end{Bmatrix} k \exp\{-k|z-h|\},$$

$$(q = x, y, \text{ or } z)$$

$$\tilde{V}^j_{32q} = \tilde{V}^j_{42q} = 0, \text{ for } z = h \tag{14}$$

for the stress vectors, where the values with upper bars in the right-hand sides of the equations are constants, which we show later how to determine.

Substituting the asymptotic solutions (13) and (14) into the corresponding displacement-stress vectors of equations (11) and (12), and by analytic integration using the relations given in Appendix C, we obtain

$$\tilde{U}^j_{r\binom{x}{y}}(r,\theta,z;h) = \left\{ \tilde{V}^j_{11\binom{x}{y}} \left(S_1 - \frac{S_4}{r} \right) + \tilde{V}^j_{12\binom{x}{y}} \left(S_2 - \frac{S_5}{r} \right) + \tilde{H}^j_{1\binom{x}{y}} \frac{S_4}{r} \right\} \begin{pmatrix} \cos\theta \\ \sin\theta \end{pmatrix} \equiv \tilde{u}^j_{r\binom{x}{y}} \begin{pmatrix} \cos\theta \\ \sin\theta \end{pmatrix}$$

$$\tilde{U}^j_{rz}(r,\theta,z;h) = -\{\tilde{V}^j_{11z} S_5 + \tilde{V}^j_{12z} S_6\}$$

$$\tilde{U}^j_{\theta\binom{x}{y}}(r,\theta,z;h) = \begin{pmatrix} - \\ + \end{pmatrix}\left\{\tilde{V}^j_{11\binom{x}{y}}\frac{S_4}{r} + \tilde{V}^j_{12\binom{x}{y}}\frac{S_5}{r} + \tilde{H}^j_{1\binom{x}{y}}\left(S_1 - \frac{S_4}{r}\right)\right\}\begin{pmatrix}\sin\theta \\ \cos\theta\end{pmatrix}$$

$$\equiv \begin{pmatrix} - \\ + \end{pmatrix}\tilde{u}^j_{\theta\binom{x}{y}}\begin{pmatrix}\sin\theta \\ \cos\theta\end{pmatrix}$$

$$\tilde{U}^j_{z\binom{x}{y}}(r,\theta,z;h) = -\{\tilde{V}^j_{21\binom{x}{y}}S_5 + \tilde{V}^j_{22\binom{x}{y}}S_6\}\begin{pmatrix}\cos\theta \\ \sin\theta\end{pmatrix}$$

$$\equiv -\tilde{u}^j_{z\binom{x}{y}}\begin{pmatrix}\cos\theta \\ \sin\theta\end{pmatrix}$$

$$\tilde{U}^j_{zz}(r,\theta,z;h) = -\{\tilde{V}^j_{21z}S_1 + \tilde{V}^j_{22z}S_2\}, \tag{15}$$

for displacement, and

$$\tilde{\sigma}^j_{rz\binom{x}{y}}(r,\theta,z;h) = \left\{\tilde{V}^j_{31\binom{x}{y}}\left(S_2 - \frac{S_5}{r}\right) + \tilde{V}^j_{32\binom{x}{y}}\left(S_3 - \frac{S_6}{r}\right) + \tilde{H}^j_{2\binom{x}{y}}\frac{S_5}{r}\right\}\begin{pmatrix}\cos\theta \\ \sin\theta\end{pmatrix}$$

$$\tilde{\sigma}^j_{rzz}(r,\theta,z;h) = -\{\tilde{V}^j_{31z}S_6 + \tilde{V}^j_{32z}S_7\}$$

$$\tilde{\sigma}^j_{\theta z\binom{x}{y}}(r,\theta,z;h) = \begin{pmatrix} - \\ + \end{pmatrix}\left\{\tilde{V}^j_{31\binom{x}{y}}\frac{S_5}{r} + \tilde{V}^j_{32\binom{x}{y}}\frac{S_6}{r} + \tilde{H}^j_{2\binom{x}{y}}\left(S_2 - \frac{S_5}{r}\right)\right\}\begin{pmatrix}\sin\theta \\ \cos\theta\end{pmatrix}$$

$$\tilde{\sigma}^j_{zz\binom{x}{y}}(r,\theta,z;h) = -\left\{\tilde{V}^j_{41\binom{x}{y}}S_6 + \tilde{V}^j_{42\binom{x}{y}}S_7\right\}\begin{pmatrix}\cos\theta \\ \sin\theta\end{pmatrix}$$

$$\tilde{\sigma}^j_{zzz}(r,\theta,z;h) = -\{\tilde{V}^j_{41z}S_2 + \tilde{V}^j_{42z}S_3\}, \tag{16}$$

for stress; see Appendix C for S_1 through S_7.

Procedure to Compute the Green's Function Using the Asymptotic Solution

We describe how to compute static and dynamic Green's functions due to point sources, using the asymptotic solutions obtained above. This procedure is basically the same as Herrmann's (1993).

First, we determine the constant values in equations (13) and (14). We obtain those values by substituting z, h, and large wavenumbers into the corresponding displacement-stress vectors given in Appendix A:

$$\tilde{H}^j_{1q} = H^j_{1q}(\bar{k})\exp\{\bar{k}|z-h|\}$$

$$\tilde{V}^j_{\binom{1}{2}2q}\begin{cases} = \dfrac{1}{\bar{k}_2 - \bar{k}_1}\{V^j_{\binom{1}{2}q}(\bar{k}_2)\exp\{\bar{k}_2|z-h|\} \\ \quad - V^j_{\binom{1}{2}q}(\bar{k}_1)\exp\{\bar{k}_1|z-h|\}\} & (z \neq h) \\ = 0, & (z = h)\end{cases}$$

$$\tilde{V}^j_{\binom{1}{2}q}\begin{cases} = V^j_{\binom{1}{2}q}(\bar{k}_1)\exp\{\bar{k}_1|z-h|\} - \bar{k}_1\tilde{V}^j_{\binom{1}{2}2q} & (z \neq h) \\ = V^j_{\binom{1}{2}q}(\bar{k}), & (z = h)\end{cases}$$

(17)

for the displacement vectors, and

$$\tilde{H}^j_{2q} = \frac{1}{\bar{k}}H^j_{2q}(\bar{k})\exp\{\bar{k}|z-h|\}$$

$$\tilde{V}^j_{\binom{3}{4}2q}\begin{cases} = \dfrac{1}{\bar{k}_2 - \bar{k}_1}\left\{\dfrac{1}{\bar{k}_2}V^j_{\binom{3}{4}q}(\bar{k}_2)\exp\{\bar{k}_2|z-h|\}\right. \\ \quad \left. - \dfrac{1}{\bar{k}_1}V^j_{\binom{3}{4}q}(\bar{k}_1)\exp\{\bar{k}_1|z-h|\}\right\} & (z \neq h) \\ = 0, & (z = h)\end{cases}$$

$$\tilde{V}^j_{\binom{3}{4}1q}\begin{cases} = \dfrac{1}{\bar{k}_1}V^j_{\binom{3}{4}q}(\bar{k}_1)\exp\{\bar{k}_1|z-h|\} - \bar{k}_1\tilde{V}^j_{\binom{3}{4}2q} & (z \neq h) \\ = \dfrac{1}{\bar{k}}V^j_{\binom{3}{4}q}(\bar{k}), & (z = h)\end{cases}$$

(18)

for the stress vectors, where $\bar{k}$, $\bar{k}_1$, and $\bar{k}_2$ are large wavenumbers much greater than the Rayleigh and Love poles and the branch points, satisfying the following conditions:

$$\bar{k}, \bar{k}_1, \text{ and } \bar{k}_2 \gg \max\{\text{real}\,(k^j_\beta \text{ or } k^j_\alpha)\}, \quad (j = 1, 2, \ldots, N+1) \tag{19}$$

and $\bar{k}_1 \neq \bar{k}_2$.

Second, subtracting asymptotic solutions (13) and (14) from the corresponding displacement-stress vectors in equations (11) and (12) and adding the analytic integrations (15) and (16) to the outsides of the integrals, we obtain the final solutions

$$U^j_{r\binom{x}{y}}(r,\theta,z;h) = \int_0^\infty \left[\{V^j_{1\binom{x}{y}} - \tilde{V}^j_{1\binom{x}{y}}\}\frac{dJ_1}{dkr} + \{H^j_{1\binom{x}{y}} - \tilde{H}^j_{1\binom{x}{y}}\}\frac{J_1}{kr}\right]dk\begin{pmatrix}\cos\theta \\ \sin\theta\end{pmatrix} + \tilde{U}^j_{r\binom{x}{y}}$$

$$U^j_{rz}(r,\theta,z;h) = -\int_0^\infty [\{V^j_{1z} - \tilde{V}^j_{1z}\}J_1(kr)]dk + \tilde{U}^j_{rz}$$

$$U^j_{\theta\binom{x}{y}}(r,\theta,z;h) = \begin{pmatrix} - \\ + \end{pmatrix} \int_0^\infty \left[\{V^j_{1\binom{x}{y}} - \tilde{V}^j_{1\binom{x}{y}}\} \frac{J_1}{kr} + \{H^j_{1\binom{x}{y}} - \tilde{H}^j_{1\binom{x}{y}}\} \frac{dJ_1}{dkr} \right] dk \begin{pmatrix} \sin\theta \\ \cos\theta \end{pmatrix} + \tilde{U}^j_{\theta\binom{x}{y}}$$

$$U^j_{z\binom{x}{y}}(r,\theta,z;h) = -\int_0^\infty [\{V^j_{2\binom{x}{y}} - \tilde{V}^j_{2\binom{x}{y}}\} J_1(kr)]dk \cdot \begin{pmatrix} \cos\theta \\ \sin\theta \end{pmatrix} + \tilde{U}^j_{z\binom{x}{y}}$$

$$U^j_{zz}(r,\theta,z;h) = -\int_0^\infty [\{V^j_{2z} - \tilde{V}^j_{2z}\} J_0(kr)]dk + \tilde{U}^j_{zz}, \quad (20)$$

for displacement, and

$$\sigma^j_{rz\binom{x}{y}}(r,\theta,z;h) = \int_0^\infty \left[\{V^j_{3\binom{x}{y}} - \tilde{V}^j_{3\binom{x}{y}}\} \frac{dJ_1}{dkr} + \{H^j_{2\binom{x}{y}} - \tilde{H}^j_{2\binom{x}{y}}\} \frac{J_1}{kr} \right] dk \begin{pmatrix} \cos\theta \\ \sin\theta \end{pmatrix} + \tilde{\sigma}^j_{rz\binom{x}{y}}$$

$$\sigma^j_{rzz}(r,\theta,z;h) = -\int_0^\infty [\{V^j_{3z} - \tilde{V}^j_{3z}\} J_1(kr)]dk + \tilde{\sigma}^j_{rzz}$$

$$\sigma^j_{\theta z\binom{x}{y}}(r,\theta,z;h) = \begin{pmatrix} - \\ + \end{pmatrix} \int_0^\infty \left[\{V^j_{3\binom{x}{y}} - \tilde{V}^j_{3\binom{x}{y}}\} \frac{J_1}{kr} + \{H^j_{2\binom{x}{y}} - \tilde{H}^j_{2\binom{x}{y}}\} \frac{dJ_1}{dkr} \right] dk \begin{pmatrix} \sin\theta \\ \cos\theta \end{pmatrix} + \tilde{\sigma}^j_{\theta z\binom{x}{y}}$$

$$\sigma^j_{zz\binom{x}{y}}(r,\theta,z;h) = -\int_0^\infty [\{V^j_{4\binom{x}{y}} - \tilde{V}^j_{4\binom{x}{y}}\} J_1(kr)]dk \cdot \begin{pmatrix} \cos\theta \\ \sin\theta \end{pmatrix} + \tilde{\sigma}^j_{zz\binom{x}{y}}$$

$$\sigma^j_{zzz}(r,\theta,z;h) = -\int_0^\infty [\{V^j_{4z} - \tilde{V}^j_{4z}\} J_0(kr)]dk + \tilde{\sigma}^j_{zzz}, \quad (21)$$

for stress. Since the { } parts in the above integrands converge to zero with increasing wavenumber, we can efficiently carry out the numerical integrations.

Green's Functions Due to Dipole Sources

We show the procedure to obtain Green's functions due to dipole sources using the asymptotic technique presented above. Those Green's functions in the frequency domain are expressed in the Cartesian coordinate system shown in Figure 1, as follows:

$$U^s_k(0,0,h) = M_{ji}U^j_{ik,j}(r,\theta,z;h) = M_{ji}U^j_{ik,j}(x,y,z;h), \quad (22)$$

where the subscripts i, j, and k are vector components in the Cartesian coordinate and the summation conventions are used for them, a comma between subscripts is used in spatial derivatives at the point (x,y,z), M_{ji} is the moment tensor (see, e.g., Aki and Richards, 1980). To make direct use of the asymptotic solutions obtained above, we do not use the reciprocity theorem in equation (22). Therefore, U^s_k is the displacement at the source location $(0,0,h)$ in the sth layer, due to the moment tensor applied at the receiver location (x,y,z) in the jth layer.

Green's functions in the cylindrical coordinate system, given in equation (11), are transferred to those in the Cartesian coordinate system as follows:

$$U^j_{xk} = U^j_{rk}\cos\theta - U^j_{\theta k}\sin\theta$$

$$U^j_{yk} = U^j_{rk}\sin\theta + U^j_{\theta k}\cos\theta. \quad (23)$$

The spatial derivatives of equation (23), which are required in equation (22), are

$$U^j_{xk,j} = U^j_{rk,j}\cos\theta + U^j_{rk}(\cos\theta)_{,j} - U^j_{\theta k,j}\sin\theta - U^j_{\theta k}(\sin\theta)_{,j}$$

$$U^j_{yk,j} = U^j_{rk,j}\sin\theta + U^j_{rk}(\sin\theta)_{,j} + U^j_{\theta k,j}\cos\theta + U^j_{\theta k}(\cos\theta)_{,j} \quad (24)$$

for $j = x$ or y, and

$$U^j_{xk,z} = U^j_{rk,z}\cos\theta - U^j_{\theta k,z}\sin\theta$$

$$U^j_{yk,z} = U^j_{rk,z}\sin\theta + U^j_{\theta k,z}\cos\theta \quad (25)$$

where

$$\cos\theta = \frac{x}{r}, \quad \sin\theta = \frac{y}{r}, \quad r = \sqrt{x^2+y^2}$$

$$(\cos\theta)_{,x} = \frac{\sin^2\theta}{r}, \quad (\sin\theta)_{,y} = \frac{\cos^2\theta}{r}$$

$$(\cos\theta)_{,y} \equiv (\sin\theta)_{,x} = -\frac{\sin\theta\cos\theta}{r}. \quad (26)$$

The spatial derivatives of Green's functions in the right-hand sides of equations (24) and (25) are obtained from equation (11)

$$U^j_{r\binom{x}{y},j} = \int_0^\infty \left\{ V^j_{1\binom{x}{y}} \left(\frac{dJ_1}{dkr}\right)_{,j} + H^j_{1\binom{x}{y}} \left(\frac{J_1}{kr}\right)_{,j} \right\} dk \begin{pmatrix}\cos\theta\\ \sin\theta\end{pmatrix} + u^j_{r\binom{x}{y}} \begin{pmatrix}\cos\theta\\ \sin\theta\end{pmatrix}_{,j}$$

$$U^j_{rz,j} = -\int_0^\infty \{V^j_{1z}(J_1)_{,j}\} dk$$

$$U^j_{\theta\binom{x}{y},j} = \begin{pmatrix}-\\ +\end{pmatrix} \left[\int_0^\infty \left\{ V^j_{1\binom{x}{y}} \left(\frac{J_1}{kr}\right)_{,j} + H^j_{1\binom{x}{y}} \left(\frac{dJ_1}{dkr}\right)_{,j} \right\} dk \cdot \begin{pmatrix}\sin\theta\\ \cos\theta\end{pmatrix} + u^j_{\theta\binom{x}{y}} \begin{pmatrix}\sin\theta\\ \cos\theta\end{pmatrix}_{,j} \right]$$

$$U^j_{z\binom{x}{y},j} = -\left[\int_0^\infty \{V^j_{2\binom{x}{y}} (J_1)_{,j}\} dk \begin{pmatrix}\cos\theta\\ \sin\theta\end{pmatrix} + u^j_{z\binom{x}{y}} \begin{pmatrix}\cos\theta\\ \sin\theta\end{pmatrix}_{,j} \right]$$

$$U^j_{zz,j} = -\int_0^\infty \{V^j_{2z} (J_0)_{,j}\} dk \tag{27}$$

for $j = x$ or y, where u^j_{pq} is defined in equation (11), and

$$\frac{dJ_1}{dkr} = J_0 - \frac{J_1}{kr}, \quad (J_0)_{,j} = -J_1 kr_{,j}, \quad (J_1)_{,j} = \frac{dJ_1}{dkr} kr_{,j}$$

$$\left(\frac{J_1}{kr}\right)_{,j} = \frac{r_{,j}}{r}\left(J_0 - 2\frac{J_1}{kr}\right),$$

$$\left(\frac{dJ_1}{dkr}\right)_{,j} = -\frac{r_{,j}}{r}\left(J_0 - 2\frac{J_1}{kr} + krJ_1\right)$$

$$r_{,x} = \cos\theta, \quad r_{,y} = \sin\theta. \tag{28}$$

We also obtain

$$U^j_{r\binom{x}{y},z} = \int_0^\infty \left\{ V^j_{1\binom{x}{y},z} \frac{dJ_1}{dkr} + H^j_{1\binom{x}{y},z} \frac{J_1}{kr} \right\} dk \begin{pmatrix}\cos\theta\\ \sin\theta\end{pmatrix}$$

$$U^j_{rz,z} = -\int_0^\infty \{V^j_{1z,z} J_1\} dk$$

$$U^j_{\theta\binom{x}{y},z} = \begin{pmatrix}-\\ +\end{pmatrix} \int_0^\infty \left\{ V^j_{1\binom{x}{y},z} \frac{J_1}{kr} + H^j_{1\binom{x}{y},z} \frac{dJ_1}{dkr} \right\} dk \begin{pmatrix}\sin\theta\\ \cos\theta\end{pmatrix}$$

$$U^j_{z\binom{x}{y},z} = -\int_0^\infty \{V^j_{2\binom{x}{y},z} J_1\} dk \begin{pmatrix}\cos\theta\\ \sin\theta\end{pmatrix}$$

$$U^j_{zz,z} = -\int_0^\infty \{V^j_{2z,z} J_0\} dk. \tag{29}$$

We obtain $H^j_{1k,z}$, $V^j_{1k,z}$, and $V^j_{2k,z}$ in equation (29) from H^j_{2k}, and V^j_{1k} through V^j_{4k} in equation (11) and (12) and Appendix A using the following relations:

$$H^j_{1k,z} = \frac{1}{\mu^j} H^j_{2k}, \quad (\text{for } k = x \text{ or } y), \tag{30}$$

and

$$V^j_{1k,z} = \frac{1}{\mu^j} V^j_{3k} + kV^j_{2k}$$

$$V^j_{2k,z} = \frac{1}{\lambda^j + 2\mu^j} \{V^j_{4k} - k\lambda^j V^j_{1k}\},$$

$$(\text{for } k = x, y, \text{ or } z), \tag{31}$$

where μ^j and λ^j are Lame's constant of the jth layer. For the derivation of the above equations for the 2D case, see equations (7.20) through (7.27) of Chapter 7 in Aki and Richards (1980). It is easy to confirm that the same relations are true for the 3D case.

Using a similar procedure used from equation (13) to (16) plus equations (30) and (31), the wavenumber integrations of the asymptotic solutions in equations (27) and (29) are analytically derived as follows:

$$\tilde{U}^j_{r\binom{x}{y},j} = r_{,j}\{-(\bar{V}^j_{11\binom{x}{y}} S_6 + \bar{V}^j_{12\binom{x}{y}} S_7) - B_{\binom{x}{y}} + A_{\binom{x}{y}}\} \cdot \begin{pmatrix}\cos\theta\\ \sin\theta\end{pmatrix} + \tilde{u}^j_{r\binom{x}{y}} \begin{pmatrix}\cos\theta\\ \sin\theta\end{pmatrix}_{,j}$$

$$\tilde{U}^j_{rz,j} = -r_{,j}\left\{ \bar{V}^j_{11z} S_2 + \bar{V}^j_{11z} S_3 - \frac{1}{r}\tilde{u}^j_{zz} \right\}$$

$$\tilde{U}^j_{\theta\binom{x}{y},j} = \begin{pmatrix}-\\ +\end{pmatrix} \left[r_{,j}\{B_{\binom{x}{y}} - \bar{H}^j_{1\binom{x}{y}} S_6 - A_{\binom{x}{y}}\} \begin{pmatrix}\sin\theta\\ \cos\theta\end{pmatrix} + \tilde{U}^j_{\theta\binom{x}{y}} \begin{pmatrix}\sin\theta\\ \cos\theta\end{pmatrix}_{,j} \right]$$

$$\tilde{U}^j_{z\binom{x}{y},j} = -\left[r_{,j} \left\{ \bar{V}^j_{21\binom{x}{y}} S_2 + \bar{V}^j_{22\binom{x}{y}} S_3 - \frac{1}{r}\tilde{u}^j_{z\binom{x}{y}} \right\} \begin{pmatrix}\cos\theta\\ \sin\theta\end{pmatrix} + \tilde{u}^j_{z\binom{x}{y}} \begin{pmatrix}\cos\theta\\ \sin\theta\end{pmatrix}_{,j} \right]$$

$$\tilde{U}^j_{zz,j} = r_{,j}\{\bar{V}^j_{21z}S_6 + \bar{V}^j_{22z}S_7\} \tag{32}$$

for $j = x$ and y, where $\tilde{u}^j_{pq}$ is defined in equation (15), and

$$A_{\binom{x}{y}} = \frac{1}{r}\bar{H}^j_{1\binom{x}{y}}\left(S_1 - \frac{2}{r}S_4\right)$$

$$B_{\binom{x}{y}} = \frac{1}{r}\left\{\bar{V}^j_{11\binom{x}{y}}\left(S_1 - \frac{2}{r}S_4\right) + \bar{V}^j_{12\binom{x}{y}}\left(S_2 - \frac{2}{r}S_5\right)\right\}. \tag{33}$$

We also obtain

$$\tilde{U}^j_{r\binom{x}{y},z} = \left\{\left(\frac{1}{\mu^j}\bar{V}^j_{31\binom{x}{y}} + \bar{V}^j_{21\binom{x}{y}}\right)\left(S_2 - \frac{S_5}{r}\right) + \left(\frac{1}{\mu^j}\bar{V}^j_{32\binom{x}{y}} + \bar{V}^j_{22\binom{x}{y}}\right)\left(S_3 - \frac{S_6}{r}\right) + \frac{1}{\mu^j}\bar{H}^j_{2\binom{x}{y}}\frac{S_5}{r}\right\}\begin{pmatrix}\cos\theta\\ \sin\theta\end{pmatrix}$$

$$\tilde{U}^j_{rz,z} = -\left\{\left(\frac{1}{\mu^j}\bar{V}^j_{31z} + \bar{V}^j_{21z}\right)S_6 + \left(\frac{1}{\mu^j}\bar{V}^j_{32z} + \bar{V}^j_{22z}\right)S_7\right\}$$

$$\tilde{U}^j_{\theta\binom{x}{y},z} = \begin{pmatrix}-\\ +\end{pmatrix}\left\{\left(\frac{1}{\mu^j}\bar{V}^j_{31\binom{x}{y}} + V^j_{21\binom{x}{y}}\right)\frac{S_5}{r} + \left(\frac{1}{\mu^j}\bar{V}^j_{32\binom{x}{y}} + \bar{V}^j_{22\binom{x}{y}}\right)\frac{S_6}{r} + \frac{1}{\mu^j}\bar{H}^j_{2\binom{x}{y}}\left(S_2 - \frac{S_5}{r}\right)\right\}\begin{pmatrix}\sin\theta\\ \cos\theta\end{pmatrix}$$

$$\tilde{U}^j_{z\binom{x}{y},z} = -\frac{1}{\lambda^j + 2\mu^j}\{(\bar{V}^j_{41\binom{x}{y}} - \lambda^j\bar{V}^j_{11\binom{x}{y}})S_6 + (\bar{V}^j_{42\binom{x}{y}} - \lambda^j\bar{V}^j_{12\binom{x}{y}})S_7\}\begin{pmatrix}\cos\theta\\ \sin\theta\end{pmatrix}$$

$$\tilde{U}^j_{zz,z} = -\frac{1}{\lambda^j + 2\mu^j}\{(\bar{V}^j_{41z} - \lambda^j\bar{V}^j_{11z})S_2 + (\bar{V}^j_{42z} - \lambda^j\bar{V}^j_{12z})S_3\} \tag{34}$$

Finally, we obtain Green's functions due to dipole sources using the following procedure. First, we determine the constants $\bar{H}^j_{pq}$ and $\bar{V}^j_{pq}$ using equations (17) and (18) and construct the asymptotic solutions (13) and (14) plus (30) and (31). Second, we subtract the asymptotic solutions from the corresponding displacement-stress vectors in equations (27) and (29), and numerically carry out the wavenumber integrations. Finally, we obtain the Green's function (22) by adding the analytical integrations (32) and (34) to the corresponding numerical integrations.

We confirmed that our Green's functions due to point and dipole sources agree well with those by a numerical code based on Haskell's propagator matrix method, which was derived from Harkrider (1964). We also confirmed that the former is much more numerically stable than the latter, although we will not show those results here because of limited space.

Results

We shall test the effectiveness of our method for various source-receiver configurations, using the model shown in Figure 2. We show here only the cases for point sources. We also have similar results for dipole sources but we do not show them because of limited space. This model consists of two layers (shear-wave velocities: β = 1 and 2 km/sec) overlying a homogeneous half-space (β = 3 km/sec). For the cases from 1 to 5, we show only the results of selected displacement-stress vectors and total integrands (the products of the displacement-stress vectors and Bessel functions) for the circular frequency (ω) = 1, since we have obtained almost same conclusions for the other cases we tried. In the final case 6, we compare the values of Green's functions obtained by the original integrations [equations (11) and (12)] with those by the use of the asymptotic solutions [equations (20) and (21)]. In all cases, except case 3, we take $\bar{k}$, $\bar{k}_1$, and $\bar{k}_2$ of equations (17) and (18) as the following values:

$$\bar{k}_1 = 50 \text{ real } (k^1_\beta) \approx 0.05,$$

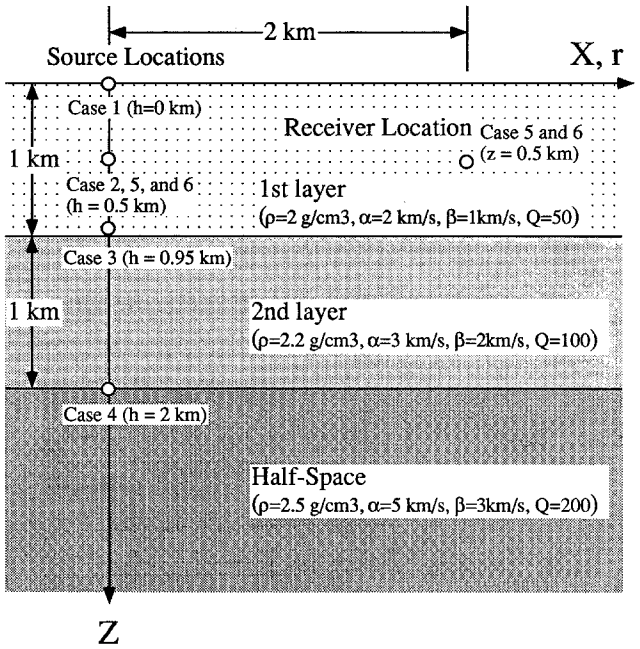

Figure 2. The layered half-space model to check our method. In the following computations, we use a point source with $Q_x = Q_y = Q_z = 1$ for the case of $\omega = 1$.

$$\bar{k} = \overline{k_2} = 60 \text{ real } (k_\beta^1) \approx 0.06$$

which are large enough to construct the asymptotic solutions (13), (14), (17), and (18).

Case 1 (Displacement-Stress Vectors for the Source on the Free Surface)

In the first case, we fix the source at the free surface ($h = 0$) and locate the receivers at two different depths ($z = 0$ and 100 m) for displacement and four depths ($z = 0$, 10, 100, and 500 m) for stress. Since the imaginary parts of the displacement-stress vectors quickly converge to zero without the use of the asymptotic technique, we only show the results of the real parts in this and the subsequent cases from 2 to 5. Figure 3 shows wavenumber versus the real parts of the displacement vector V_{2z}^j. Solid lines represent the original vector V_{2z}^j, and the dashed and dotted lines correspond to the vector with the asymptotic technique ($V_{2z}^j - \tilde{V}_{2z}^j$), which is referred as "our method" in the figure. When the source and the receiver are located at the same depth ($h = z = 0$), the original vector V_{2z}^j converges to a constant as the wavenumber increases beyond the peaks and troughs corresponding to the Rayleigh poles. When the receiver depth is close to the source depth, the same vector slowly decreases as an exponential function. These properties are expected from equation (13) and Appendix B. In contrast, the vector by our method ($V_{2z}^j - \tilde{V}_{2z}^j$) quickly converges to zero in all cases.

Similarly, Figure 4 shows the stress vector V_{4z}^j. Solid lines represent the original vector V_{4z}^j and the other kinds of lines correspond to the vector $V_{4z}^j - \tilde{V}_{4z}^j$ for various depths of the receiver. When the source and the receiver are located at the same depth, the original vectors diverge, as expected from equation (14) and Appendix B. However, the vector by our method quickly converges to zero for all cases.

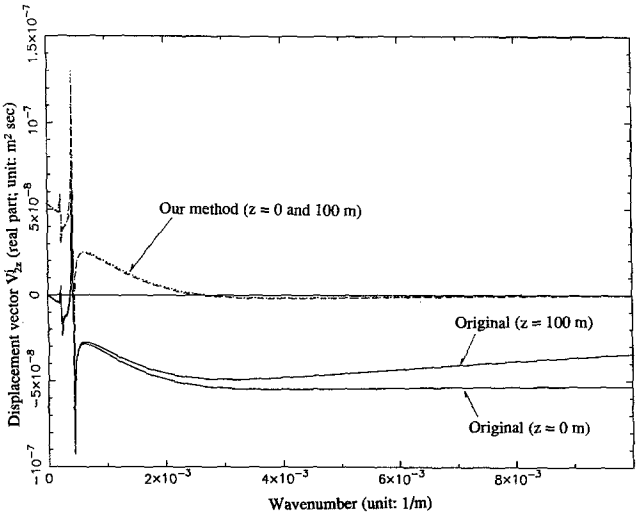

Figure 3. Wavenumber versus the real parts of the displacement vector V_{2z}^j for case 1 (the source depth, $h = 0$). The solid lines represent the original vector V_{2z}^j, and the dashed and dotted lines show the vector by our method ($V_{1x}^j - \tilde{V}_{1x}^j$). Note that the dashed and dotted lines share almost identical trajectories, and quickly converge to zero with increasing wavenumber.

Case 2 (Displacement-Stress Vectors for the Source at the Middle of a Layer)

In this case, we fix the source at the middle of the first-layer ($h = 500$ m) and take the receiver at various depths. Because we obtained the almost same results to those of the case 1, we show just one stress vector. Figure 5 shows the original vector V_{4x}^j, and the vector $V_{4x}^j - \tilde{V}_{4x}^j$. Similarly to case 1, the latter quickly converges to zero beyond the Rayleigh poles.

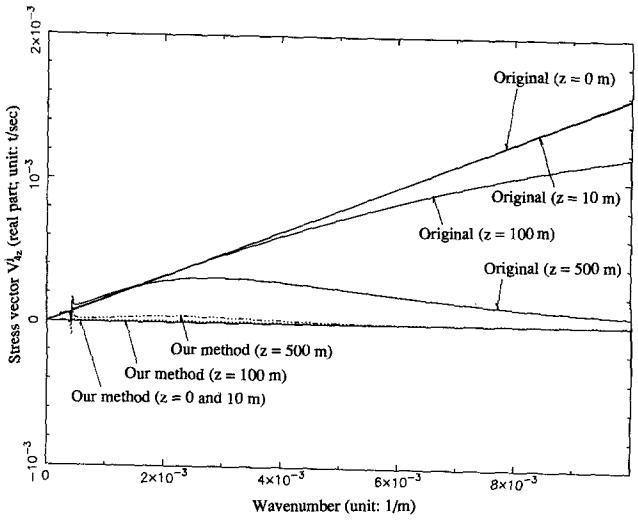

Figure 4. Same as Figure 3 but for the stress vector V_{4z}^j.

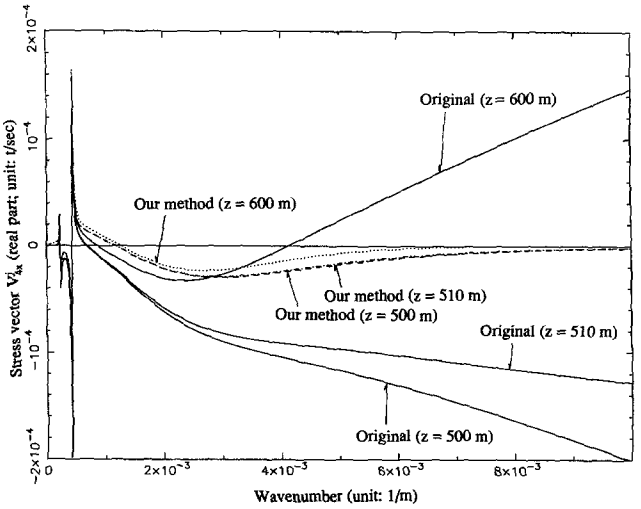

Figure 5. Same as Figure 3 but for the stress vector V_{4x}^j in case 2 ($h = 500$ m).

Case 3 (Displacement-Stress Vectors for the Source Close to a Boundary between Layers)

In our third case, we fix the source 50 m above the first boundary (h = 950 m) and locate the receivers at two different depths (z = 950 and 1050 m) for displacement and three depths (z = 950, 960, and 1050 m) for stress. Note that the receiver at z = 1050 m is located in a different layer from the source layer. We found that the values for $\bar{k}$, $\bar{k}_1$, and $\bar{k}_2$ given earlier were not large enough to construct the asymptotic solutions (13) and (14), because of the waves reflected from the boundary close to the source, which are neglected in the solutions. Thus, we use the following larger values in this case:

$$\bar{k}_1 = 200 \text{ real } (k_\beta^1) \approx 0.20,$$

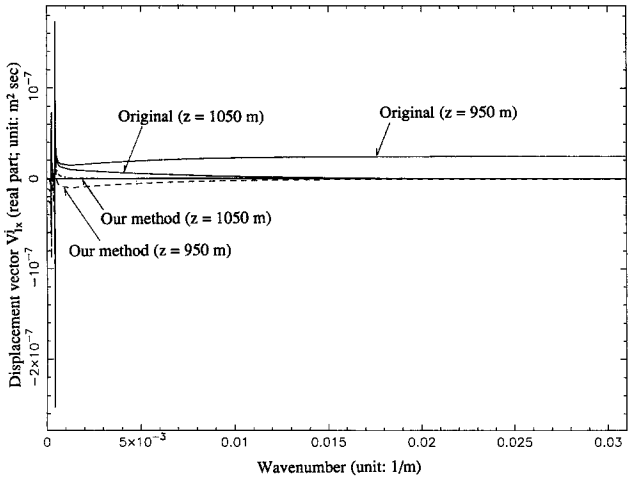

Figure 6. Same as Figure 3 but for the displacement vector V_{1x}^j in case 3 (h = 950 m).

$$\bar{k} = \bar{k}_2 = 210 \text{ real } (k_\beta^1) \approx 0.21.$$

Figure 6 shows the displacement vector V_{1x}^j and $V_{1x}^j - \tilde{V}_{1x}^j$. Similarly, Figure 7 shows those of stress vector V_{4x}^j. Although both vectors by our method ($V_{1x}^j - \tilde{V}_{1x}^j$ and $(V_{4x}^j - \tilde{V}_{4x}^j)$ converge to zero much more quickly than the originals (V_{1x}^j and $\tilde{V}_{4x}^j$), even for z = 1050 m, the rates of convergence are much slower than the previous two cases; note that the scales of the horizontal axes in the two figures are larger than those in the previous figures. As mentioned above, this is because of the reflected waves; their amplitudes converge slowly to zero with wavenumber in this case, as shown in equation (B3) and (B4) in Appendix B.

Case 4 (Displacement-Stress Vectors for the Source on a Boundary between Layers)

We check the case for the source located on the boundary between the second layer and the underlying half-spaces (h = 2000 m). All displacement-stress vectors quickly converge to zero. As an example, Figure 8 shows the case for a stress vector. This indicates the validity of equations (13) and (14) in this case.

Case 5 (Total Integrands of Green's Functions)

Next, we show the total integrands of Green's functions given in equations (11), (12), (20), and (21), which are expressed by the products of the displacement-stress vectors and Bessel functions. We choose the case for h = 500 m, r = 2000 m, θ = 0, and $Q_x = Q_y = Q_z = 1$. Figure 9 plots the integrand of U_{zz}^1 against wavenumber for z = 500 and 550 m. The solid lines represent the original integrands, and the dashed and dotted lines correspond to the integrands minus the asymptotic solutions for z = 500 and 550 m, respectively. The solid lines oscillate with slowly decaying amplitudes, whereas the

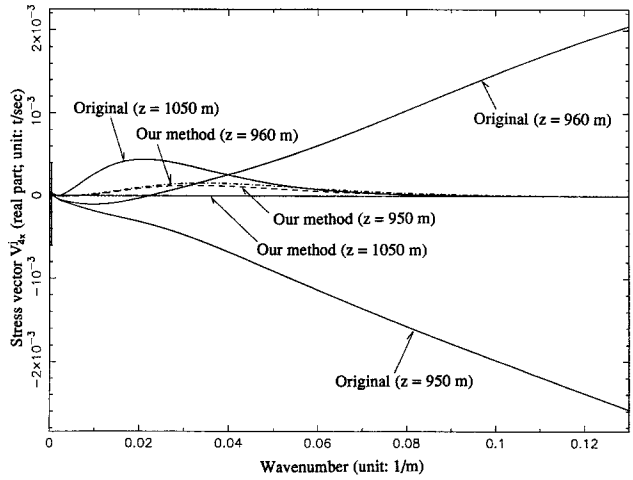

Figure 7. Same as Figure 6 but for the stress vector V_{4x}^j.

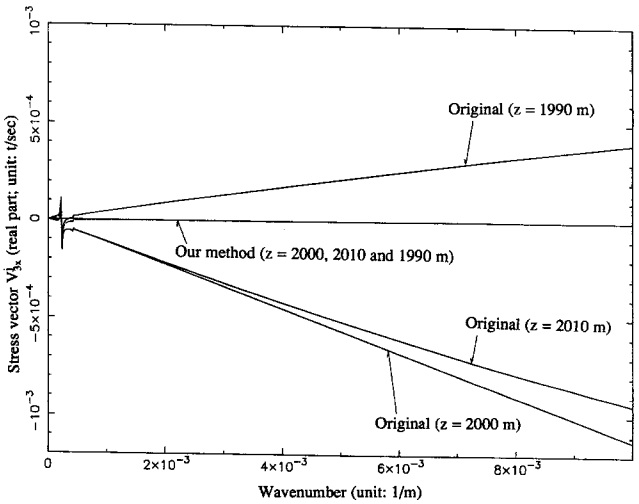

Figure 8. Same as Figure 3 but for the stress vector V_{3x}^j in case 4 (h = 2000 m).

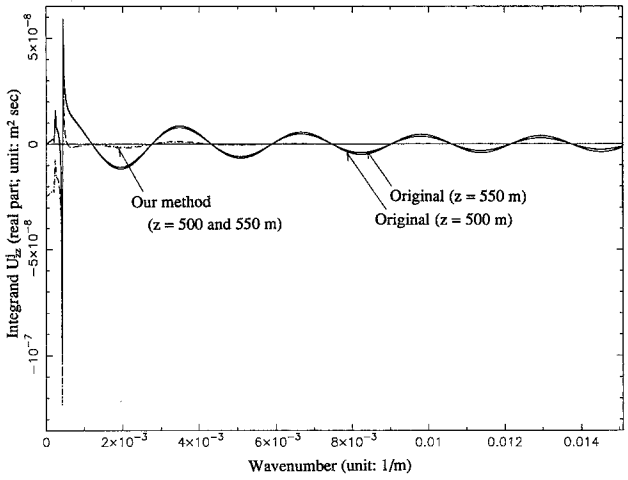

Figure 9. Wavenumber versus the real parts of the integrand U^1_{zz} for case 5 (h = 500 m). The solid lines and the broken lines represent the results by the original and our methods, respectively. The integrands by the original method show slowly decreasing oscillations with wavenumber, whereas those by our method show quick convergence to zero.

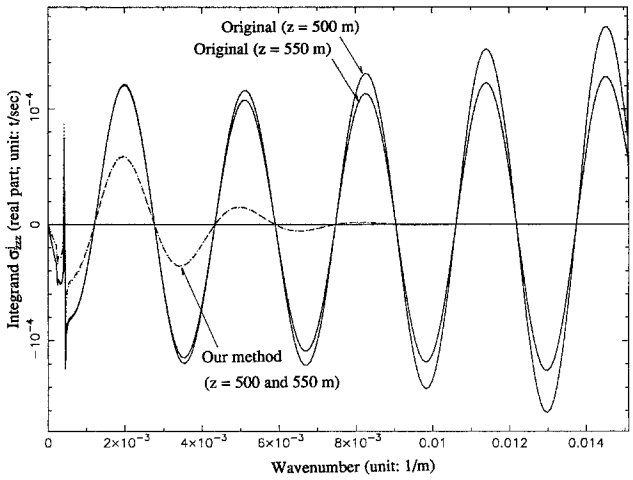

Figure 10. Same as Figure 9 but for σ^1_{zzz}. The integrands by the original method show increasing oscillations with wavenumber, while those by our method show quickly decreasing oscillations.

dashed and dotted lines quickly converge to zero. Similarly, Figure 10 shows the integrand of σ^j_{zzz}. The original integrand for z = 500 m has an increasing-oscillation, which is very difficult to integrate numerically, as shown in case 6. The original integrand for z = 550 m has an extremely slowly decreasing oscillation. On the contrary, the integrands minus the asymptotic solutions (dashed and dashed lines) quickly converge to zero for all cases, which can be easily integrated.

Case 6 (Green's Functions by the Original Integration versus Those by Our Method)

Finally, we compare the final values of Green's functions obtained by the original integrations [equations (11) and (12)] and those by the use of the asymptotic technique [equations (20) and (21)]. We adopt the same parameters used in case 5 and carry out the numerical integrations using Simpson's rule with increments of 0.000001 for wavenumbers between 0.000001 and 0.0006, and with increments of 0.0001 for wavenumbers greater than 0.0006. We can use the larger increments beyond 0.0006, because of the smooth oscillations of the integrands beyond the Love and Rayleigh poles, as seen in Figures 9 and 10.

Figure 11 shows the upper limit of the integration range (maximum wavenumber) versus the absolute values of the three displacement components, $|U^1_{rx} + U^1_{ry} + U^1_{rz}|$, $|U^1_{\theta x} + U^1_{\theta y} + U^1_{\theta z}|$, and $|U^1_{zx} + U^1_{zy} + U^1_{zz}|$, and the stresses components, $|\sigma^1_{rzx} + \sigma^1_{rzy} + \sigma^1_{rzz}|$, $|\sigma^1_{\theta zx} + \sigma^1_{\theta zy} + \sigma^1_{\theta zz}|$, and $|\sigma^1_{zzx} + \sigma^1_{zzy} + \sigma^1_{zzz}|$, for the case of z = 500 m. We computed those values using both the original integration method and our proposed method. The displacements by our method show faster and more stable convergence with increasing upper limit. The stresses by our method quickly converge as the upper limit increases, whereas those by the original method diverge. Similarly, Figure 12 shows the displacements and stresses in the case of z = 550 m. Again, we see much faster convergences in the results by our method, especially for the stresses.

Conclusions

We have proposed an efficient method for computing the static and dynamic Green's functions for a layered half-space with sources and receivers at close depths. We considered both point and dipole sources. There are two main elements in this method. First, we can express Green's functions as the sum of two integrals, one being soluble analytically and the other needing numerical computation. Second, we can do efficient numerical integrations, because the integrands converge quickly to zero as the wavenumber increases. We have compared our method to others to confirm that our method can significantly reduce the range of wavenumber integration for all cases we tried.

Acknowledgments

The author is grateful to X. Chen, B.-H. Chin, K. Aki, and D. Adams for valuable discussions, particularly to D. Adams for improving the English of the manuscript. Comments by R. B. Herrmann and an anonymous referee were also helpful in the revision of this manuscript. This work was in part supported by the Kajima Foundation's Research Grant, NSF under Contract ACS-9318163, and Southern California Earthquake Center through NSF cooperative agreement EAR-8920136 and USGS cooperative agreement through 14-08-0001-A0899.

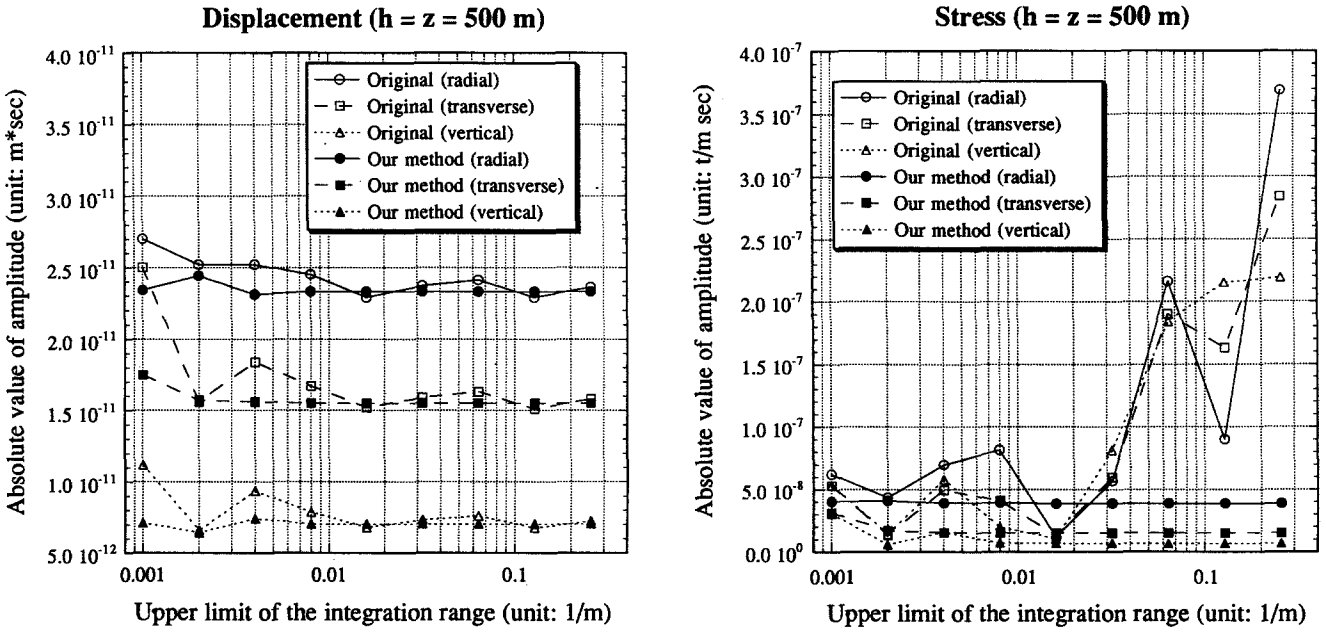

Figure 11. The relations between the upper limit of the integration range and the absolute values of the displacement and stress components of Green's functions, for case 6 ($h = z = 500$ m). The results by our method show much faster convergence than those by the original method. In particular, note that the stresses by the original method diverge with increasing upper limits.

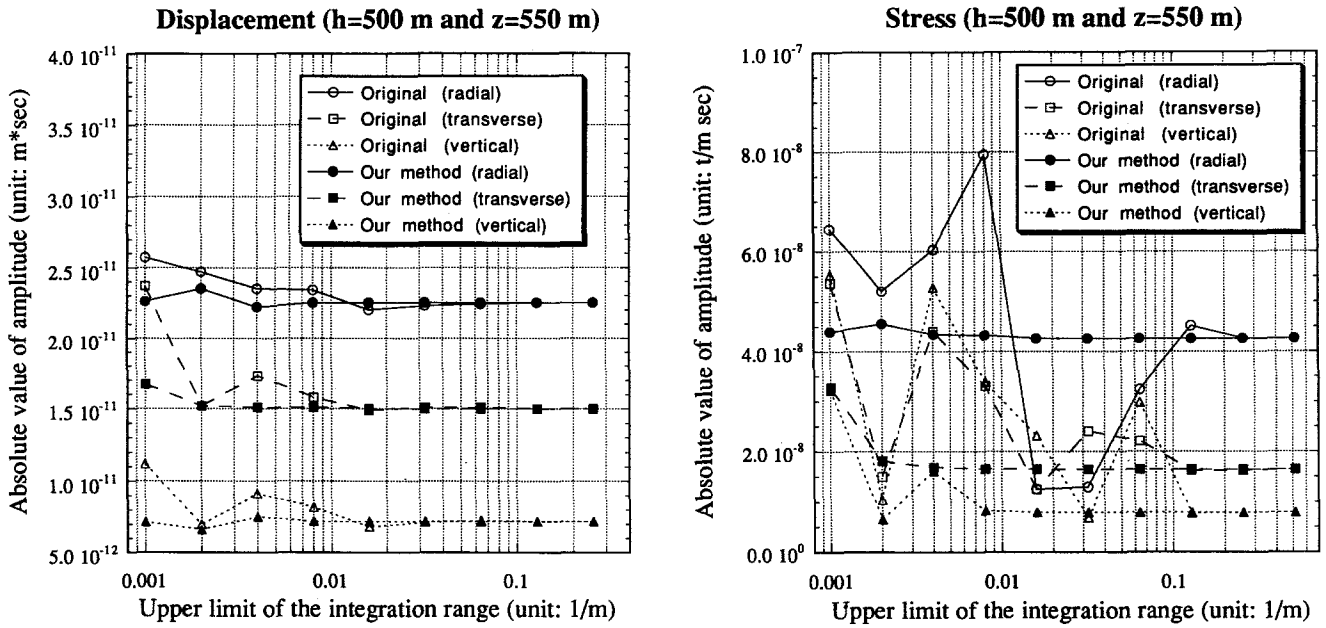

Figure 12. Same as Figure 11 but for the case of $z = 550$ m. Again, the results by our method show much faster convergence.

References

Aki, K. and P. G. Richards (1980). *Quantitative Seismology, Theory and Methods*, Vol. 1, W. H. Freeman.

Apsel, R. J. and J. E. Luco (1983). On the Green's functions for a layered half-space, part 2, *Bull. Seism. Soc. Am.* **73**, 931–951.

Chang, S. (1988). Complete wavefield modeling and seismic inversion for lossy-elastic layered half-space due to surface force, *Ph.D. Thesis*, University of Southern California, Los Angeles.

Chen, X. (1993). A systematic and efficient method of computing normal modes for multilayered half-space, *Geophys. J. Int.* **115**, 391–409.

Chin, B.-H. (1992). Simultaneous study of the source, path and site effects on strong ground motion during the 1989 Loma Prieta

earthquake, *Ph.D. Thesis*, University of Southern California, Los Angeles.

Harkrider, D. G. (1964). Surface waves in multilayered elastic media; Rayleigh and Love waves from buried sources in a multilayered elastic half-space, *Bull. Seism. Soc. Am.* **54**, 627–679.

Haskell, N. A. (1953). The dispersion of surface waves on multilayered media, *Bull. Seism. Soc. Am.* **43**, 17–34.

Haskell, N. A. (1964). Radiation pattern of surface waves from point sources in a multilayered medium, *Bull. Seism. Soc. Am.* **54**, 377–394.

Herrmann, R. B. and C. Y. Wang (1985). A comparison of synthetic seismograms, *Bull. Seism. Soc. Am.* **75**, 41–56.

Herrmann, R. B. (1993). Elastic wave Green's functions for isotropic layered media, in "Quantification of m_{Lg} for small explosions," Final Report PL-TR-93-2070, Phillips Laboratory, Hanscom Air Force Base, Massachusetts.

Kennett, B. L. N. (1974). Reflections, ray, and reverberations, *Bull. Seism. Soc. Am.* **64**, 1685–1696.

Kennett, B. L. N. and N. J. Kerry (1979). Seismic waves in a stratified half space, *Geophys. J. R. Astr. Soc.* **57**, 557–583.

Luco, J. E. and R. J. Apsel (1983). On the Green's functions for a layered half-space, part 1, *Bull. Seism. Soc. Am.* **73**, 909–929.

Appendix A
Dynamic and Static Displacement-Stress Vectors

We show here the dynamic and static displacement-stress vectors in equations (11) and (12), which are completely free from the exponentials growing with wavenumber and/or frequency. We derive them using the generalized R/T coefficient method (Luco and Apsel, 1983) and the stress discontinuity (Harkrider, 1964) to express the boundary and source conditions, respectively.

The dynamic displacement-stress vectors of the jth layer (V^j_{pq} and H^j_{pq}) are expressed by the downgoing and upgoing P and S waves in the following matrix form:

$$\begin{Bmatrix} D^j(z;h) \\ S^j(z,h) \end{Bmatrix} = \begin{bmatrix} E^j_{11} & E^j_{12} \\ E^j_{21} & E^j_{22} \end{bmatrix} \begin{bmatrix} \Lambda^j_d(z) & 0 \\ 0 & \Lambda^j_u(z) \end{bmatrix} \begin{Bmatrix} C^j_d(h) \\ C^j_u(h) \end{Bmatrix}, \tag{A1}$$

where

$$D^j(z;h) = \begin{Bmatrix} V^j_{1q}(z;h) \\ V^j_{2q}(z;h) \end{Bmatrix}, \quad S^j(z;h) = \begin{Bmatrix} V^j_{3q}(z;h) \\ V^j_{4q}(z;h) \end{Bmatrix},$$

$$(q = x, y \text{ or } z) \tag{A2}$$

$$C^j_d(h) = \begin{Bmatrix} c^j_{d\alpha}(h) \\ c^j_{d\beta}(h) \end{Bmatrix}, \quad C^j_u(h) = \begin{Bmatrix} c^j_{u\alpha}(h) \\ c^j_{u\beta}(h) \end{Bmatrix} \tag{A3}$$

$$\begin{bmatrix} E^j_{11} & E^j_{12} \\ E^j_{21} & E^j_{22} \end{bmatrix} = \begin{bmatrix} -1 & \gamma^j_\beta & -1 & \gamma^j_\beta \\ -\gamma^j_\alpha & 1 & \gamma^j_\alpha & -1 \\ 2\mu^j\nu^j_\alpha & -\mu^j\chi^j & -2\mu^j\nu^j_\alpha & \mu^j\chi^j \\ \mu^j\chi^j & -2\mu^j\nu^j_\beta & \mu^j\chi^j & -2\mu^j\nu^j_\beta \end{bmatrix} \tag{A4}$$

$$\Lambda^j_d(z) = \begin{bmatrix} \exp\{-\nu^j_\alpha(z - z^{(j-1)})\} & 0 \\ 0 & \exp\{-\nu^j_\beta(z - z^{(j-1)}\} \end{bmatrix}$$

$$\Lambda^j_u(z) = \begin{bmatrix} \exp\{-\nu^j_\alpha(z^{(j)} - z)\} & 0 \\ 0 & \exp\{-\nu^j_\beta(z^{(j)} - z)\} \end{bmatrix} \tag{A5}$$

$$\nu^{j2}_\alpha = k^2 - k^{j2}_\alpha,$$

$$(\mathrm{Re}\,\{\nu^j_\alpha\} \geqq 0, \quad k^j_\alpha = \omega/\bar{\alpha}^j, \quad \bar{\alpha}^j = \alpha^j(1 - i/2Q^j_\alpha))$$

$$\nu^{j2}_\beta = k^2 - k^{j2}_\beta,$$

$$(\mathrm{Re}\,\{\nu^j_\beta\} \geqq 0, \quad k^j_\beta = \omega/\bar{\beta}^j, \quad \bar{\beta}^j = \beta^j(1 - i/2Q^j_\beta))$$

$$\gamma^j_\alpha = \nu^j_\alpha/k, \quad \gamma^j_\beta = \nu^j_\beta/k, \quad \chi^j = 2k - k^{j2}_\beta/k \tag{A6}$$

for the *P-SV* wave, and

$$D^j(z;h) = H^j_{1q}(z;h),$$

$$S^j(z;h) = H^j_{2q}(z;h), \quad (q = x \text{ or } y) \tag{A7}$$

$$C^j_d(h) = c^j_{d\beta}(h), \quad C^j_u(h) = c^j_{u\beta}(h) \tag{A8}$$

$$\begin{bmatrix} E^j_{11} & E^j_{12} \\ E^j_{21} & E^j_{22} \end{bmatrix} = \begin{bmatrix} 1 & 1 \\ -\mu^j\nu^j_\beta & \mu^j\nu^j_\beta \end{bmatrix} \tag{A9}$$

$$\Lambda^j_d(z) = \exp\{-\nu^j_\beta(z - z^{(j-1)})\},$$

$$\Lambda^j_u(z) = \exp\{-\nu^j_\beta(z^{(j)} - z)\} \tag{A10}$$

for the *SH* wave. In equation (A6), α^j and Q^j_α are the P-wave velocity and the quality factor of the P wave of the jth layer, respectively, and β^j and Q^j_β are those of the S wave. Note that the definition of (A4) is different from those of Luco and Apsel (1983) or equation (7.55) in Aki and Richards (1980), because of the difference of the normalization of the down/upgoing coefficients (A3).

In the case of the static displacement-stress vectors ($\omega = 0$), we need to modify equations (A4) through (A10). Following the same procedure from equations (53) to (60) in Luco and Apsel (1983), we obtain

$$\begin{bmatrix} E^j_{11} & E^j_{12} \\ E^j_{21} & E^j_{22} \end{bmatrix} = \begin{bmatrix} 1 & 1 & 1 & 1 \\ -(\kappa^j - 1) & 1 & (\kappa^j - 1) & -1 \\ k\,\mu^j(\kappa^j - 3) & -2k\,\mu^j & -k\,\mu^j(\kappa^j - 3) & 2k\,\mu^j \\ k\,\mu^j(\kappa^j - 1) & -2k\,\mu^j & k\,\mu^j(\kappa^j - 1) & -2k\,\mu^j \end{bmatrix}$$

$$\kappa^j = \frac{1 + (\bar{\beta}^j/\bar{\alpha}^j)^2}{1 - (\bar{\beta}^j/\bar{\alpha}^j)^2} \tag{A11}$$

$$\Lambda_d^j(z) = \begin{bmatrix} 1 & 0 \\ -k(z - z^{(j-1)}) & 1 \end{bmatrix} \exp\{-k(z - z^{(j-1)})\}$$

$$\Lambda_u^j(z) = \begin{bmatrix} 1 & 0 \\ -k(z^{(j)} - z) & 1 \end{bmatrix} \exp\{-k(z^{(j)} - z)\} \tag{A12}$$

for the *P-SV* wave, and

$$\begin{bmatrix} E_{11}^j & E_{12}^j \\ E_{21}^j & E_{22}^j \end{bmatrix} = \begin{bmatrix} 1 & 1 \\ -\mu^j k & \mu^j k \end{bmatrix} \tag{A13}$$

$$\Lambda_d^j(z) = \exp\{-k(z - z^{(j-1)})\},$$

$$\Lambda_u^j(z) = \exp\{-k(z^{(j)} - z)\} \tag{A14}$$

for the *SH* wave.

In equation (A1), the down/upgoing coefficients C_d^j and C_u^j are determined from the source and boundary conditions. In the following, we divide our formulation into three cases.

Case 1 (the Down/Upgoing Coefficients for $h \neq 0$ and $h \leqq z^{(N-1)}$)

We first present the down/upgoing coefficients, in the case of $h \neq 0$ and $h \leqq z^{(N-1)}$ (the source is located neither on the free surface nor in the underlying half-space). In this case, we divide the source layer (sth layer) into the upper (S^-) and lower (S^+) layer at the source depth h, and consider them as two individual layers (see Fig. 1).

First, since the downgoing waves only exist in the underlying half-space ($j = N + 1$), we get

$$C_u^{N+1} = \{0\}. \tag{A15}$$

Second, we define the modified R/T coefficients $T_d^{(j)}$, $R_d^{(j)}$, $T_u^{(j)}$, and $R_u^{(j)}$ (Luco and Apsel, 1983) for the jth boundary between the jth and $j + 1$th layers

$$C_n^j = R_d^{(j)} C_d^j + T_u^{(j)} C_u^{j+1}$$

$$C_d^{j+1} = T_d^{(j)} C_d^j + R_u^{(j)} C_u^{j+1},$$

$$(\text{for } j = 1, 2, \ldots, N). \tag{A16}$$

For the free surface ($j = 0$), since the reflection coefficients only exists, we define

$$C_d^1 = R_u^{(0)} C_u^1. \tag{A17}$$

Using equation (A1) for the jth and $j + 1$th layers and considering the continuity conditions of displacement and stress, we obtain the modified R/T coefficients defined above as follows:

$$R_u^{(0)} = -(E_{21}^1)^{-1} E_{22}^1 \Lambda_u^1(0)$$

$$\begin{bmatrix} T_d^{(j)} & R_u^{(j)} \\ R_d^{(j)} & T_u^{(j)} \end{bmatrix} = \begin{bmatrix} E_{11}^{j+1} & -E_{12}^j \\ E_{21}^{j+1} & -E_{22}^j \end{bmatrix}^{-1} \begin{bmatrix} E_{11}^j & -E_{12}^{j+1} \\ E_{21}^j & -E_{22}^{j+1} \end{bmatrix}$$

$$\begin{bmatrix} \Lambda_d^j(z^{(j)}) & 0 \\ 0 & \Lambda_u^{j+1}(z^{(j)}) \end{bmatrix},$$

$$(\text{for } j = 1, 2, \ldots, N - 1)$$

$$\begin{Bmatrix} T_d^{(N)} \\ R_d^{(N)} \end{Bmatrix} = \begin{bmatrix} E_{11}^{N+1} & -E_{12}^N \\ E_{21}^{N+1} & -E_{22}^N \end{bmatrix}^{-1} \begin{Bmatrix} E_{11}^N \Lambda_d^N(z^{(N)}) \\ E_{21}^N \Lambda_d^N(z^{(N)}) \end{Bmatrix}. \tag{A18}$$

Third, we define the generalized R/T coefficients $\tilde{T}_d^{(j)}$, $\tilde{R}_d^{(j)}$, $\tilde{T}_u^{(j)}$, and $\tilde{R}_u^{(j)}$ (Luco and Apsel, 1983) as follows:

$$C_u^j(h) = \tilde{T}_u^{(j)} C_u^{j+1}(h), \quad C_d^{j+1}(h) = \tilde{R}_u^{(j)} C_u^{j+1}(h),$$

$$(\text{for } j = 1, \ldots, S - 1) \tag{A19}$$

$$C_d^{j+1}(h) = \tilde{T}_d^{(j)} C_d^j(h), \quad C_u^j(h) = \tilde{R}_d^{(j)} C_d^j(h),$$

$$(\text{for } j = N - 1, \ldots, S), \tag{A20}$$

where S is the source layer. We can derive the generalized R/T coefficients from the modified R/T coefficients using the following recurrence relations:

$$\tilde{R}_u^{(0)} = R_u^{(0)}, \quad (\text{for } j = 0)$$

$$\tilde{T}_u^{(j)} = (I - R_d^{(j)} \tilde{R}_u^{(j-1)})^{-1} T_u^{(j)}$$

$$\tilde{R}_u^{(j)} = R_u^{(j)} + T_d^{(j)} \tilde{R}_u^{(j-1)} \tilde{T}_u^{(j)},$$

$$(\text{for } j = 1, \ldots, S - 1) \tag{A21}$$

for the layers upper than the source, and

$$\tilde{T}_d^{(N)} = T_d^{(N)}, \quad \tilde{R}_d^{(N)} = R_d^{(N)}, \quad (\text{for } j = N)$$

$$\tilde{T}_d^{(j)} = (I - R_u^{(j)} \tilde{R}_d^{(j+1)})^{-1} T_d^{(j)}$$

$$\tilde{R}_d^{(j)} = R_d^{(j)} + T_u^{(j)} \tilde{R}_d^{(j+1)} \tilde{T}_d^{(j)},$$

$$(\text{for } j = N - 1, \ldots, S) \tag{A22}$$

for the layers lower than the source. I is the identity matrix.

Fourth, in order to obtain the down/upgoing coefficients of the Sth layer, we introduce "the stress discontinuities" (Harkrider, 1964) at the boundary between the S^- and S^+ layers to express the source conditions

$$\begin{Bmatrix} D^{S+}(h) \\ S^{S+}(h) \end{Bmatrix} = \begin{Bmatrix} D^{S-}(h) \\ S^{S-}(h) \end{Bmatrix} + \begin{Bmatrix} 0 \\ \Delta Q_q \end{Bmatrix}, \quad (q = x, y, \text{or } z) \tag{A23}$$

where

$$\Delta Q_x = \begin{Bmatrix} -\frac{k}{2\pi} Q_x \\ 0 \end{Bmatrix}, \quad \Delta Q_y = \begin{Bmatrix} -\frac{k}{2\pi} Q_y \\ 0 \end{Bmatrix}$$

$$\Delta Q_z = \begin{Bmatrix} 0 \\ \frac{k}{2\pi} Q_z \end{Bmatrix} \tag{A24}$$

for the *P-SV* wave, and

$$\Delta Q_x = -\frac{k}{2\pi} Q_x, \quad \Delta Q_y = -\frac{k}{2\pi} Q_y \tag{A25}$$

for the *SH* wave. Using equation (A1) for the S^- and S^+ layers and considering (A23), we finally obtain the down/upgoing coefficients of the two layers

$$\begin{aligned} C_u^{S-}(h) &= (B^{S+} D^S - B^{S-})^{-1} \Delta Q_q, \quad (q = x, y, \text{or } z) \\ C_d^{S+}(h) &= D^S C_u^{S-}(h), \\ C_d^{S-}(h) &= \tilde{R}_u^{(S-1)} C_u^{S-}(h), \\ C_u^{S+}(h) &= \tilde{R}_d^{(S)} C_d^{S+}(h), \end{aligned} \tag{A26}$$

where

$$\begin{aligned} A^{S-} &= E_{11}^S \Lambda_d^{S-}(h) \tilde{R}_u^{(S-1)} + E_{12}^S, \\ A^{S+} &= E_{11}^S + E_{12}^S \Lambda_u^{S+}(h) \tilde{R}_d^{(S)} \\ B^{S-} &= E_{21}^S \Lambda_d^{S-}(h) \tilde{R}_u^{(S-1)} + E_{22}^S, \\ B^{S+} &= E_{21}^S + E_{22}^S \Lambda_u^{S+}(h) \tilde{R}_d^{(S)} \\ D^S &= (A^{S+})^{-1} A^{S-}. \end{aligned} \tag{A27}$$

Finally, we obtain the down/upgoing coefficients of all layers by substituting (A26) into (A19) and (A20).

Case 2 (the Down/Upgoing Coefficients for $h = 0$)

When the source is located on the free surface ($S = 1$ and $h = 0$), we need to slightly modify our formulation. We first derive all modified and generalized R/T coefficients using equations (A18) and (A22), respectively. Second, instead of (A23), we use the following source condition:

$$S^1(h = 0) = \Delta Q_q, \quad (q = x, y, \text{or } z). \tag{A28}$$

Substituting (A28) and (A20) in equation (A1) of the first layer, we get the downgoing coefficient in the first layer

$$C_d^1 = (E_{21}^1 + E_{22}^1 \Lambda_u^1(0) \tilde{R}_d^{(1)})^{-1} \Delta Q_q, \quad (q = x, y, \text{or } z). \tag{A29}$$

All the other coefficients are obtained by (A20).

Case 3 (the Down/Upgoing Coefficients for $h \geqq z^{(N-1)}$)

When the source is located in the underlying half-space ($S = N + 1$ and $h \geqq z^{(N)}$), we first divide the underlying half-space into the upper layer ($N + 1^-$) and the lower half-space ($N + 1^+$) at the source depth, and then derive the modified and generalized R/T coefficients for all boundaries between adjacent layers using equations (A18) and (A21). Second, we introduce "the stress discontinuities" at the boundary, as done in (A23).

$$\begin{Bmatrix} D^{N+1^+}(h) \\ S^{N+1^+}(h) \end{Bmatrix} = \begin{Bmatrix} D^{N+1^-}(h) \\ S^{N+1^-}(h) \end{Bmatrix} + \begin{Bmatrix} 0 \\ \Delta Q_q \end{Bmatrix}, \quad (q = x, y, \text{or } z). \tag{A30}$$

In the lower half-space ($N + 1^+$), since only the downgoing waves exist,

$$C_u^{N+1^+} = \{0\}. \tag{A31}$$

Using equation (A1) for the $N + 1^-$ and $N + 1^+$ layers and considering (A30) and (A31), we finally obtain the down/upgoing coefficients of the two layers

$$\begin{aligned} C_u^{N+1^-}(h) &= (B^{N+1^+} D^{N+1^-} - B^{N+1^-})^{-1} \Delta Q_q, \\ &\quad (q = x, y, \text{or } z) \\ C_d^{N+1^+}(h) &= D^{N+1} C_u^{N+1^-}(h), \end{aligned} \tag{A32}$$

where

$$\begin{aligned} A^{N+1^-} &= E_{11}^{N+1} \Lambda_d^{N+1^-}(h) \tilde{R}_u^{(N)} + E_{12}^{N+1}, \quad A^{N+1^+} = E_{11}^{N+1}, \\ B^{N+1^-} &= E_{21}^{N+1} \Lambda_d^{N+1^-}(h) \tilde{R}_u^{(N)} + E_{22}^{N+1}, \quad B^{N+1^+} = E_{21}^{N+1}, \\ D^{N+1} &= (A^{N+1^+})^{-1} A^{N+1^-}. \end{aligned} \tag{A33}$$

The all other coefficients are obtained from (A19).

Appendix B
Asymptotic Solutions of the Displacement-Stress Vectors

We derive the asymptotic solutions of the displacement-stress vectors at large wavenumbers, using the

equations given in Appendix A. Since the dynamic displacement-stress vectors converge to the static ones with increasing wavenumber as shown in Luco and Apsel (1983), we use the static displacement-stress vectors in the following.

As k tends toward infinity, the highest orders of k in equation (A11) and (A13) are

$$E^j_{11} \text{ and } E^j_{12} \to o(k^0),$$
$$E^j_{21} \text{ and } E^j_{22} \to o(k^1). \tag{B1}$$

Those in (A12) and (A14) are

$$\Lambda^j_d \to o(k^0) \text{ (for } z = z^{(j-1)}) \text{ or } 0 \text{ (for } z \neq z^{(j-1)}),$$
$$\Lambda^j_u \to o(k^0) \text{ (for } z = z^{(j)}) \text{ or } 0 \text{ (for } z \neq z^{(j)}). \tag{B2}$$

Case 1 (the Down/Upgoing Coefficients for $h \neq 0$ and $h \leqq z^{(N-1)}$)

From (B1) and (B2), we find the modified R/T coefficients given in (A18) converge to zero with increasing wavenumber

$$R^{(0)}_u \to 0,$$
$$T^{(j)}_d, R^{(j)}_u, T^{(j)}_u, \text{ and } R^{(j)}_d \to 0, \quad (j = 1, 2, \ldots, N-1)$$
$$T^{(N)}_d \text{ and } R^{(N)}_d \to 0. \tag{B3}$$

Therefore, the generalized R/T coefficients given in (A21) and (A22) also

$$\tilde{R}^{(0)}_u \to 0,$$
$$\tilde{T}^{(j)}_d, \tilde{R}^{(j)}_u, \tilde{T}^{(j)}_u, \text{ and } \tilde{R}^{(j)}_d \to 0, \quad (j = 1, 2, \ldots, N-1)$$
$$\tilde{T}^{(N)}_d \text{ and } \tilde{R}^{(N)}_d \to 0. \tag{B4}$$

This indicates that the amplitudes of all the reflected and transmitted waves from boundaries converge to zero with wavenumber.

On the other hand, the highest orders of k of the source term in (A24) and (A25) are

$$\Delta Q_q \to o(k^1), \ (q = x, y, \text{ and } z). \tag{B5}$$

Using (B2) and (B4), those of the coefficients in (A27) are

$$A^{S-} \to E^S_{12} \to o(k^0), \quad A^{S+} \to E^S_{11} \to o(k^0),$$
$$B^{S-} \to E^S_{22} \to o(k^1), \quad B^{S+} \to E^S_{21} \to o(k^1),$$
$$D^S \to o(k^0). \tag{B6}$$

Therefore, the orders of the down/upgoing coefficients of the S^- and S^+ layers in (A26) are

$$C^{S-}_u \to o(k^0), \ C^{S+}_d \to o(k^0),$$
$$C^{S-}_d \to 0, \quad C^{S+}_u \to 0. \tag{B7}$$

Substituting (B1) and (B7) into (A1) of the S^- and S^+ layers, we get the highest orders of k of the displacement-stress vectors in the source layers

$$\begin{Bmatrix} D^{S-}(z;h) \\ S^{S-}(z,h) \end{Bmatrix} \to \begin{bmatrix} o(k^0)\ o(k^0) \\ o(k^1)\ o(k^1) \end{bmatrix} \begin{bmatrix} \Lambda^{S-}_d(z) & 0 \\ 0 & \Lambda^{S-}_u(z) \end{bmatrix} \begin{Bmatrix} 0 \\ o(k^0) \end{Bmatrix}$$
$$\to \begin{Bmatrix} o(k^0)\ \Lambda^{S-}_u(z) \\ o(k^1)\ \Lambda^{S-}_u(z) \end{Bmatrix},$$
$$\begin{Bmatrix} D^{S+}(z;h) \\ S^{S+}(z,h) \end{Bmatrix} \to \begin{bmatrix} o(k^0)\ o(k^0) \\ o(k^1)\ o(k^1) \end{bmatrix} \begin{bmatrix} \Lambda^{S+}_d(z) & 0 \\ 0 & \Lambda^{S+}_u(z) \end{bmatrix} \begin{Bmatrix} 0 \\ o(k^0) \end{Bmatrix}$$
$$\to \begin{Bmatrix} o(k^0)\ \Lambda^{S+}_u(z) \\ o(k^1)\ \Lambda^{S+}_u(z) \end{Bmatrix}. \tag{B8}$$

Case 2 (the Down/Upgoing Coefficients for $h = 0$)

Similarly, we obtain the highest orders of k of the displacement-stress vectors in the source layer (the first layer)

$$\begin{Bmatrix} D^1(z;h) \\ S^1(z,h) \end{Bmatrix} \to \begin{bmatrix} o(k^0)\ o(k^0) \\ o(k^1)\ o(k^1) \end{bmatrix} \begin{bmatrix} \Lambda^1_d(z) & 0 \\ 0 & \Lambda^1_u(z) \end{bmatrix} \begin{Bmatrix} 0 \\ o(k^0) \end{Bmatrix}$$
$$\to \begin{Bmatrix} o(k^0)\ \Lambda^1_d(z) \\ o(k^1)\ \Lambda^1_d(z) \end{Bmatrix}. \tag{B9}$$

Case 3 (the Down/Upgoing Coefficients for $h \geq z^{(N-1)}$)

Similarly, we obtain

$$\begin{Bmatrix} D^{N+1^-}(z;h) \\ S^{N+1^-}(z,h) \end{Bmatrix} \to \begin{bmatrix} o(k^0)\ o(k^0) \\ o(k^1)\ o(k^1) \end{bmatrix} \begin{bmatrix} \Lambda^{N+1^-}_d(z) & 0 \\ 0 & \Lambda^{N+1^-}_u(z) \end{bmatrix}$$
$$\cdot \begin{Bmatrix} 0 \\ o(k^0) \end{Bmatrix} \to \begin{Bmatrix} o(k^0)\ \Lambda^{N+1^-}_u(z) \\ o(k^1)\ \Lambda^{N+1^-}_u(z) \end{Bmatrix},$$
$$\begin{Bmatrix} D^{N+1^+}(z;h) \\ S^{N+1^+}(z;h) \end{Bmatrix} \to \begin{Bmatrix} o(k^0)\ \Lambda^{N+1^+}_d(z)\ o(k^0) \\ o(k^1)\ \Lambda^{N+1^+}_d(z)\ o(k^0) \end{Bmatrix}$$
$$\to \begin{Bmatrix} o(k^0)\ \Lambda^{N+1^+}_d(z) \\ o(k^1)\ \Lambda^{N+1^+}_d(z) \end{Bmatrix}. \tag{B10}$$

Using the equations from (B8) to (B10) and (A12) and (A14), we can summarize the asymptotic solutions of the displacement-stress vectors for the source layer in the following forms:

$$\begin{Bmatrix} V_{1 \text{ or } 2}^{S- \text{ or } +} \\ V_{3 \text{ or } 4}^{S- \text{ or } +} \end{Bmatrix} \rightarrow \begin{Bmatrix} \bar{A} + k|z-h|\,\bar{B} \\ k(\bar{C} + k|z-h|\bar{D}) \end{Bmatrix} \exp\{-k|z-h|\},$$

(for *P-SV* wave)

$$\begin{Bmatrix} H_1^{S- \text{ or } +} \\ H_2^{S- \text{ or } +} \end{Bmatrix} \rightarrow \begin{Bmatrix} \bar{E} \\ k\bar{F} \end{Bmatrix} \exp\{-k|z-h\}. \quad \text{(for } SH \text{ wave)} \tag{B11}$$

where $\bar{A}$ through $\bar{F}$ are constant values.

From (B11), we see that the displacement vectors converge and the stress vectors increase linearly with k, in the case of $z = h$, while all displacement-stress vectors slowly converge to zero as exponential functions in the case z close to h. On the other hand, when the receiver z is located in a layer other than the source layer, the displacement-stress vectors converge more quickly to zero. This is because the all R/T coefficients converge to zero, as seen in (B3) and (B4).

Appendix C

In order to obtain equations (15) and (16), we use the following relations. Most of those are easily derived by differentiating equation (5) with respect to z and/or r.

$$S_1 \equiv \frac{1}{R} = \int_0^\infty [\exp\{-k|z-h|\}\, J_0(kr)]\, dk$$

$$S_2 \equiv \frac{|z-h|}{R^3} = \int_0^\infty [\exp\{-k|z-h|\}\, kJ_0(kr)]\, dk$$

$$S_3 \equiv \left\{3\frac{(z-h)^2}{R^2} - 1\right\}\frac{1}{R^3} = \int_0^\infty [\exp\{-k|z-h|\}\, k^2 J_0(kr)]\, dk$$

$$S_4 \equiv \frac{R-|z-h|}{r} = \int_0^\infty \left[\exp\{-k|z-h|\}\frac{J_1(kr)}{k}\right] dk$$

$$S_5 \equiv \frac{R-|z-h|}{rR} = \int_0^\infty [\exp\{-k|z-h|\}\, J_1(kr)]\, dk$$

$$S_6 \equiv \frac{r}{R^3} = \int_0^\infty [\exp\{-k|z-h|\}\, kJ_1(kr)]\, dk$$

$$S_7 \equiv 3\frac{r|z-h|}{R^5} = \int_0^\infty [\exp\{-k|z-h|\}\, k^2 J_1(kr)]\, dk$$

where $R = \sqrt{r^2 + (z-h)^2}$.

Department of Earth Sciences
University of Southern California
Los Angeles, California 90089-0740

Manuscript received 12 August 1993.